



# Zirconium–lignosulfonate polyphenolic polymer for highly efficient hydrogen transfer of biomass-derived oxygenates under mild conditions

Shenghui Zhou<sup>a</sup>, Fanglin Dai<sup>a</sup>, Zhouyang Xiang<sup>a</sup>, Tao Song<sup>a</sup>, Detao Liu<sup>a,\*</sup>, Fachuang Lu<sup>a,b</sup>, Haisong Qi<sup>a,b,\*</sup>

<sup>a</sup> State Key Laboratory of Pulp and Paper Engineering, South China University of Technology, Guangzhou 510641, China

<sup>b</sup> Department Guangdong Engineering Research Center for Green Fine Chemicals, Guangzhou 510640, China

## ARTICLE INFO

### Keywords:

Lignosulfonate-derived catalyst  
Catalytic transfer hydrogenation  
Biomass valorization  
Biofuels  
Heterogeneous catalysis

## ABSTRACT

Both value-added utilization of low-rank renewable feedstocks to prepare catalytic materials and selective transformation of bioderived aldehydes are very attractive topics. Herein, lignosulfonate, a waste by-product from the paper industry, was simply assembled with  $\text{ZrCl}_4$  under non-toxic hydrothermal conditions for scalable preparation of Zr-containing polyphenolic biopolymer catalysts (Zr–LS). Systematic characterizations indicated that the strong coordination between  $\text{Zr}^{4+}$  and phenolic hydroxyl groups in lignosulfonate led to the formation of strong Lewis acid–base couple sites ( $\text{Zr}^{4+} - \text{O}^{2-}$ ) and porous inorganic–organic framework structure (mesopores centered at 6.1 nm), while the inherent sulfonic groups in lignosulfonate could serve as Brønsted acidic sites. The cooperative role of these versatile acid–base sites in Zr–LS afforded excellent catalytic performance for Meerwein–Ponndorf–Verley (MPV) reaction of a broad range of bioderived platform chemicals under mild conditions (80 °C), especially of furfural (FF) to furfuryl alcohol (FA), in quantitative yields (96%) with high FA formation rate of  $9600 \mu\text{mol g}^{-1} \text{h}^{-1}$  and TOF of  $4.37 \text{ h}^{-1}$ . Kinetic studies revealed that the activation energy of the MPV reduction of FF was as low as 52.25 kJ/mol, accounting for the high reaction rate. Isotopic labelling experiments demonstrated direct hydrogen transfer from the  $\alpha$ -C of 2-PrOH to the  $\alpha$ -C of FF on acid–base sites was the rate-determining step. Moreover, Zr–LS showed good recyclability for at least seven reaction cycles.

## 1. Introduction

The over-exploitation and consumption of non-renewable fossil energy in traditional chemical industry have been leading to aggravating energy crisis, global warming and severe environmental pollution [1]. The utilization and transformation of lignocellulosic biomass (cellulose, hemicellulose, and lignin) is an alternative approach to provide renewable materials, valuable bio-fuels and green chemicals in the future [2–6]. In recent years, catalytic conversion of inexhaustible biomass-based chemicals (e.g., 5-hydroxymethylfurfural (5-HMF), furfural (FF), levulinic acid, glycerol, sorbitol, xylitol) have aroused particular interest [7–13]. Among these platform compounds, FF and 5-HMF can be directly obtained from hemicellulose and cellulose and have been widely used in the bio-industry to manufacture a variety of value-added products through various reactions [14–17]. Especially, selective reduction of FF and 5-HMF into furfuryl alcohol (FA) and 2,5-bis-(hydroxymethyl)-furan (BHMF) is of great application value in biorefinery. Because, FA and BHMF are important industrial intermediates widely utilized in producing artificial fibers,

pharmaceuticals, crown ethers, furan-based resins, adhesives or the production of liquid biofuels [18–20].

The Meerwein–Ponndorf–Verley (MPV) reaction is an ideal reduction technique for biomass-derived aldehydes, which furnishes a very promising alternative to dangerous gaseous hydrogen by using abundant and safe "sacrificial" alcohols as H-donor [21,22]. Various catalysts based on metal alkoxides, metal complexes, hydrotalcites, metal oxides or hydroxides, metal–organic hybrids and various zeolites have been applied for MPV reduction of biomass-based carbonyl compounds with alcohols [23,24]. Among these catalysts, abundant Zr-containing catalysts (e.g., zirconium oxide [25],  $\text{ZrO}(\text{OH})_2$  [20], zirconium phosphate [26], Zr-beta zeolites [27], Zr-based metal–organic frameworks [28], zirconium alkoxides [29]) are widely used. But there are still some inevitable shortcomings for these catalysts, such as complex preparation process, high cost of nonrenewable raw materials, high reaction temperature, long reaction time or low selectivity of target products [24]. Most recently, Zr-based inorganic–organic hybrid materials have been developed by assembling a variety of organic ligands (e.g. *meta*-xylylenediphosphonates [30], nitrilotris(methylene)

\* Corresponding authors at: State Key Laboratory of Pulp and Paper Engineering, South China University of Technology, Guangzhou 510641, China.

E-mail addresses: [dtliu@scut.edu.cn](mailto:dtliu@scut.edu.cn) (D. Liu), [qih@scut.edu.cn](mailto:qih@scut.edu.cn) (H. Qi).

<https://doi.org/10.1016/j.apcatb.2019.02.011>

Received 13 November 2018; Received in revised form 12 January 2019; Accepted 7 February 2019

Available online 07 February 2019

0926-3373/ © 2019 Elsevier B.V. All rights reserved.

triphosphonic acid [31], 4-hydroxybenzoic acid dipotassium salt [32], cyanuric acid [33]) with  $\text{Zr}^{4+}$ . Nevertheless, undesirable employment of high-toxic organic solvents (e.g., *N,N*-dimethylformamide), complex preparation process or high cost in organic ligands may limited its practical application. More importantly, a large number of organic ligands are synthesized from fossil fuel sources. Therefore, the raw materials for preparing catalysts are non-renewable. Consequently, it is desirable and imperative to explore more efficient, cost-effective and sustainable catalysts for MPV reductions of bioderived aldehydes. Recently, several Zr-containing inorganic–organic hybrid materials using natural sources (e.g., phytic acid [24], humic acids [34] and 2,5-furandicarboxylate [35,36]) as building blocks were reported for the transformation of ethyl levulinate into  $\gamma$ -valerolactone. These reports indicate that construction of catalysts from natural materials has huge potential for practical applications due to the cost advantages, non-toxicity and sustainability.

Lignin is the second most abundant lignocellulosic biomass fraction after cellulose in nature and shows great application potential owing to its inexpensiveness, accessibility, biodegradability and sustainability [4,37]. Industrial lignin, including lignosulfonate and alkali lignin, is one of the major waste by-products from the pulp and paper industry. Traditionally, most of industrial lignin is directly combusted as a low-value fuel. There's no doubt that this process could lead to serious environmental pollution. Only a minority of lignin is used to produce chemicals or biomass-based materials [38]. Thus, the development of high-value applications of industrial lignin is one of the most important directions of both modern biorefinery and the pulping industry [39]. Lignosulfonate or sulfonated lignin (LS) is abundantly found in black liquor from sulfite pulping process. Sodium sulfite or sodium bisulfite were employed in this process to remove lignin, resulting in the by-products of soluble lignosulfonates (Fig. S1) [40]. As an amphiphilic biopolymer, lignosulfonate has been widely used in the fields of concrete additive, dispersant, modifier, carbon materials, plasterboard, corrosion inhibitor or surfactant during the past few years [41]. Recently, researchers found that lignosulfonate can be used to prepare macro/mesoporous solid acids catalysts by pyrolysis process and proton exchanging. This carbon material was a highly effective catalyst for acetalization of glycerol [40]. However, the application of lignosulfonate as a ligand in catalyst synthesis is seldom reported. Due to the existence of abundant active functional groups (phenolic hydroxyl groups, alcohol hydroxyl and sulfonic groups) in its molecular structure, LS is soluble in water of varied pH and it can coordinate with various metal ions to form metal-biopolymer hybrid material.

In this contribution, we aim to prepare a novel zirconium-lignosulfonate polyphenolic polymer catalyst (Zr–LS) by using paper industry waste LS as raw materials. The fabrication process only involves a facile, nontoxic and scalable hydrothermal synthesis (Scheme 1). We performed extensive characterizations to demonstrate the formation of strong acid-base catalytic sites and robust inorganic-organic framework in Zr–LS through strong coordination interaction between zirconium and phenolic hydroxyl group. The Zr–LS was explored to be highly efficient for MPV reactions of a variety of bioderived carbonyl compounds to alcohols with 2-propanol (2-PrOH) at low temperature. To elucidate the relationship between catalytic active sites and their catalytic performance, optimizations of reaction parameter and kinetic experiments were conducted. To further investigate the FF reduction mechanism by Zr–LS, deuterium isotope tracing experiments, in combination with GC–MS analysis and *ex situ*  $^1\text{H}$  NMR technique were carried out as well. Moreover, heterogeneity, leaching and recycling experiments were also performed. We anticipate that the results will open new possibilities for exploring low-cost, environmentally friendly, renewable catalytic materials from low-rank lignosulfonate for biomass transformation.

## 2. Experimental section

### 2.1. Reagents

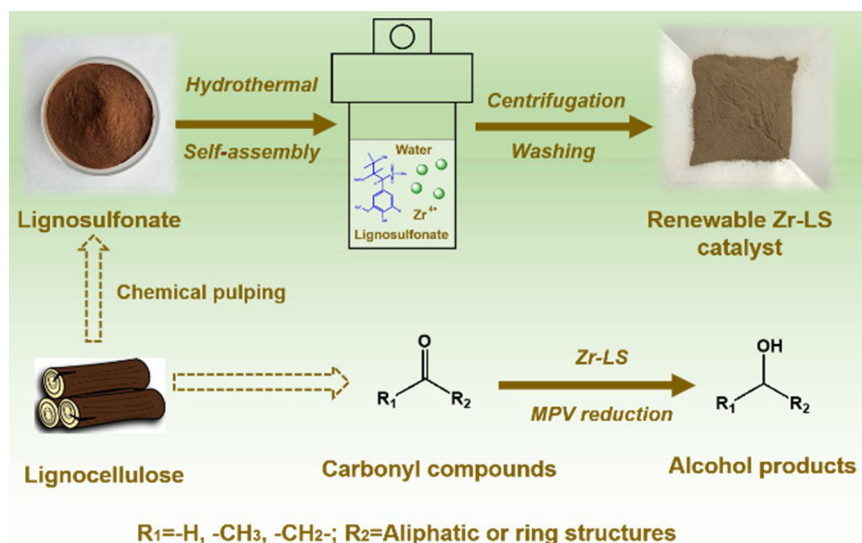
Sodium ligninsulfonate (LS, > 99.0%),  $\text{ZrCl}_4$  (> 99.5%), furfural (FF, > 99.5%), 5-hydroxymethylfurfural (HMF, > 99.0%), 5-methylfurfural (> 99.0%), citral (> 97%), cinnamaldehyde (> 99.5%), veratraldehyde (> 99.0%), ethyl levulinate (> 99.0%), *p*-anisaldehyde (> 99.5%), propanal (> 99.5%), butyraldehyde (> 99.5%), cyclopentanone (> 99.0%), cyclohexanecarboxaldehyde (> 99.0%), cyclohexanone (> 99.0%), benzaldehyde (> 99.0%), 2-hexanone (> 99.0%), phenylacetaldehyde (> 99.5%), acetophenone (> 99.0%), methanol (> 99.5%), ethanol (> 99.5%), 1-propanol (> 99.0%), 2-propanol (2-PrOH, > 99.0%), 2-butanol (> 99.0%), *tert*-butanol (> 99.0%) and 3-pentanol (> 99.0%) were purchased from Aladdin Industrial Corporation. Terephthalic acid (> 99%),  $\text{ZrO}_2$  (> 99.0%),  $\text{Zr}(\text{OH})_4$  (> 99.0%),  $\text{ZrSO}_4$  (> 98.0%) and  $\text{ZrOCl}_2$  (> 98.0%) were purchased from Shanghai Macklin Biochemical Co., Ltd, China. 2-propanol-OD (2-PrOH-OD, > 98.0%) and 2-propanol-d8 (2-PrOH-d8, > 99.0%) were purchased from Sigma-Aldrich Industrial Corporation. All chemical reagents were obtained from commercial suppliers and used without further purification.

### 2.2. Preparation of catalysts

In a typical procedure,  $\text{ZrCl}_4$  (5 g) and sodium lignosulfonate (5 g) were respectively dissolved in 15 ml and 50 ml water to form aqueous solution under ultrasound for 5 min. Subsequently, these two solutions were mixed and stirred with magnetic stirrer at room temperature for 15 min. Afterwards, the mixture was transferred into a 100 ml Teflon-lined stainless-steel autoclave and tightly sealed. This autoclave was placed into an oven that had been heated to 120 °C. After hydrothermal reaction for 12 h, the autoclave was taken out and cooled to room temperature by running water. The as-obtained brown precipitates (Fig. S2a) were centrifuged and totally washed with water for 15–20 times and ethanol for 2 times to remove the excess  $\text{ZrCl}_4$  or lignosulfonate. After the filtrate was neutral, colourless and transparent, the obtained sample was dried in vacuum at 60 °C for 12 h to afford about 6 g Zr–LS (1:1) catalyst (Fig. S2b). For the sake of reading, we abbreviate Zr–LS (1:1) as Zr–LS in the whole paper. Other Zr-lignosulfonate hybrids were prepared by changing the initial  $\text{ZrCl}_4$ /lignosulfonate mass ratios of 0.5:1, 1.5:1 and 2:1. These catalysts were designated as Zr–LS (0.5:1), Zr–LS (1.5:1) and Zr–LS (2:1) respectively. For comparison, a conventional UiO-66 (Zr) metal organic framework material was synthesised by solvothermal treatment of zirconium tetrachloride and terephthalic acid in *N,N*-dimethylformamide at 120 °C in an oven for 24 h, according to a previously reported literature [36]. Zr-HAs and Zr-SBA-15 were also prepared according to the previous reports [34,42].

### 2.3. Catalyst characterization

Scanning electron microscopy (SEM) was performed on a MERLIN SEM of ZEISS to observe the surface morphologies of different prepared catalysts. Transmission electron microscope (TEM) was conducted on a JEM-2100F with EDX analysis operated at accelerating voltage of 200 kV to observe the morphology and elemental mapping of different catalysts.  $\text{N}_2$  adsorption–desorption isotherms of different catalysts were obtained from a Micromeritics ASAP 2020 equipment. Before testing, all the catalysts were degassed at 120 °C for 6 h. Powder X-ray diffraction patterns (XRD) of different catalysts were conducted using Rigaku diffractometer (D/MAX/III A) with  $\text{Cu K}\alpha$  radiation ( $\lambda = 1.543 \text{ \AA}$ ) at ambient temperature from 5 °C to 90 °C. Fourier transform infrared spectroscopy (FT-IR) spectra of various catalysts were recorded using a Bruker Vector 33 spectrometer. The thermal stability of different samples was examined using a Mettler Toledo thermal analyser (TG) with temperature from 28 to 740 °C under



**Scheme 1.** The synthesis process of Zr-LS using lignosulfonate as the building block and its application in MPV reduction of lignocellulose-derived oxygenates.

flowing Ar (heating rate of 15 K min<sup>-1</sup>). Diffuse reflectance UV-vis (UV-vis DRS) of solid samples were obtained on an UV-2550 spectrophotometry using barium sulfate as background standard to confirm the coordination effect. Pyridine adsorbed FT-IR spectra of different catalysts were obtained on a Nicolet 380 equipment using KBr pellets in the range of 4000–400 cm<sup>-1</sup> to determine the type of acid sites. The amount of Brönsted acid sites was calculated according to 1550 cm<sup>-1</sup> characteristic band and the amount of Lewis acid sites was calculated according to 1450 cm<sup>-1</sup> characteristic band. X-ray photoelectron spectroscopy (XPS) of various samples were examined on imaging photoelectron spectrometer (Kratos Axis Ultra DLD system) under ultrahigh vacuum. The acidity and basicity of different samples were determined through temperature-programmed desorption of NH<sub>3</sub> and CO<sub>2</sub> (NH<sub>3</sub>/CO<sub>2</sub>-TPD) by a Micromeritics AutoChem II 2920 equipment. Firstly, the catalyst was degassed under a flowing He (30 mL/min) at 150 °C for 2 h. Then, the system was cooled to ambient temperature under He. After the sample was adsorbed with NH<sub>3</sub> or CO<sub>2</sub>, the system was purged under a flow of He at 50 °C and the TPD results were obtained from 50 °C to 300 °C under flowing He. The zirconium and sulfur contents in the catalysts and the solution were determined with an ICP-OES equipment (Spectro Arcos FHX22).

#### 2.4. Procedures for the MPV reduction of aldehydes

The MPV reduction reaction of aldehyde was carried out in a 25 mL pressure tube reactor (Beijing Synthware Glass Co. Ltd.) under oil-heating conditions. Typically, aldehyde (1 mmol), 2-PrOH (10 mL), and catalyst (100 mg) were added into the reactor. After that, the reactor was transferred into a preheated oil bath. After magnetically stirring for a desired time, this reactor was rapidly placed in running water. The reaction mixtures were centrifuged and collected for analysis. Identification of products was conducted using GC-MS (GCMS-QP2010 Ultra) equipped with HP-5MS capillary column (30.0 m × 250 mm × 0.25 mm). The quantification of reduction products was conducted on GC (Shimadzu Nexis GC-2030) equipped with FID detector and HP-5 capillary column (30.0 m × 250 mm × 0.25 mm).

#### 2.5. Isotopic labelling experiments

For isotopic kinetic study of MPV reduction of FF to FA, we used different deuterated 2-PrOH (2-PrOH-d8 and 2-PrOH-OD) as hydrogen source to reveal the reaction mechanism and the rate-determining step. After the reaction, the reaction mixtures were analyzed by GC-MS

(Agilent 7890B-5977A) and <sup>1</sup>H NMR (JEOL-ECX 500 NMR).

#### 2.6. Leaching experiment

In the leaching experiment, the catalyst was filtered out from the reaction system after reacting for 20 min at 100 °C. Afterwards, the FF reduction reaction was allowed to react for another 160 min under identical conditions without Zr-LS catalyst. The Zr and S species leached into the reaction mixture were analyzed by ICP-OES.

#### 2.7. Catalyst recycling experiment

The reusability test of Zr-LS catalyst was performed as follows: After the reaction proceeded at 80 °C for 1 h, the solid Zr-LS was separated by centrifugation, and washed several times with 2-PrOH. After dried under vacuum at 70 °C for 10 h, the Zr-LS was employed for the next cycle directly under the identical reaction conditions.

### 3. Results and discussion

#### 3.1. Characterization of catalysts

The structure, chemical composition, morphology and physical-chemical properties about different catalysts were characterized by several techniques. SEM and TEM revealed that Zr-LS was composed of connected irregular nanoparticles with a size range from 80 to 120 nm (Fig. 1a–d). The inserted EDS in image Fig. 1d exhibited a strong zirconium signal in Zr-LS after the coordination interaction of Zr<sup>4+</sup> with -Ar-OH in LS. The corresponding elemental mappings from HAADF-STEM in Fig. 1e and f confirmed the even dispersion and connectivity of -Ar-OH and Zr<sup>4+</sup> and homogeneous spatial arrangement of Zr, O, C and S elements throughout Zr-LS.

Furthermore, N<sub>2</sub> adsorption/desorption isotherms showed that Zr-LS displayed a typical II-type isotherm with an obvious adsorption-desorption hysteresis loop (Fig. 2a), indicating that the prepared Zr-LS was porous [43]. Table S1 showed that UiO-66 (Zr) possessed the largest surface area (1115.7 m<sup>2</sup> g<sup>-1</sup>) and pore volume (0.62 m<sup>3</sup> g<sup>-1</sup>) with the smallest average pore size (2.2 nm) calculated from N<sub>2</sub> adsorption-desorption. LS and ZrO<sub>2</sub> possessed low specific surface area and pore volume. In contrast, Zr-LS had medium BET surface area (115.15 m<sup>2</sup> g<sup>-1</sup>), pore volume (0.18 cm<sup>3</sup> g<sup>-1</sup>) and average pore diameter (6.1 nm), respectively. The larger average pore sizes can improve the diffusion of reaction substrates in pores and accessibility of

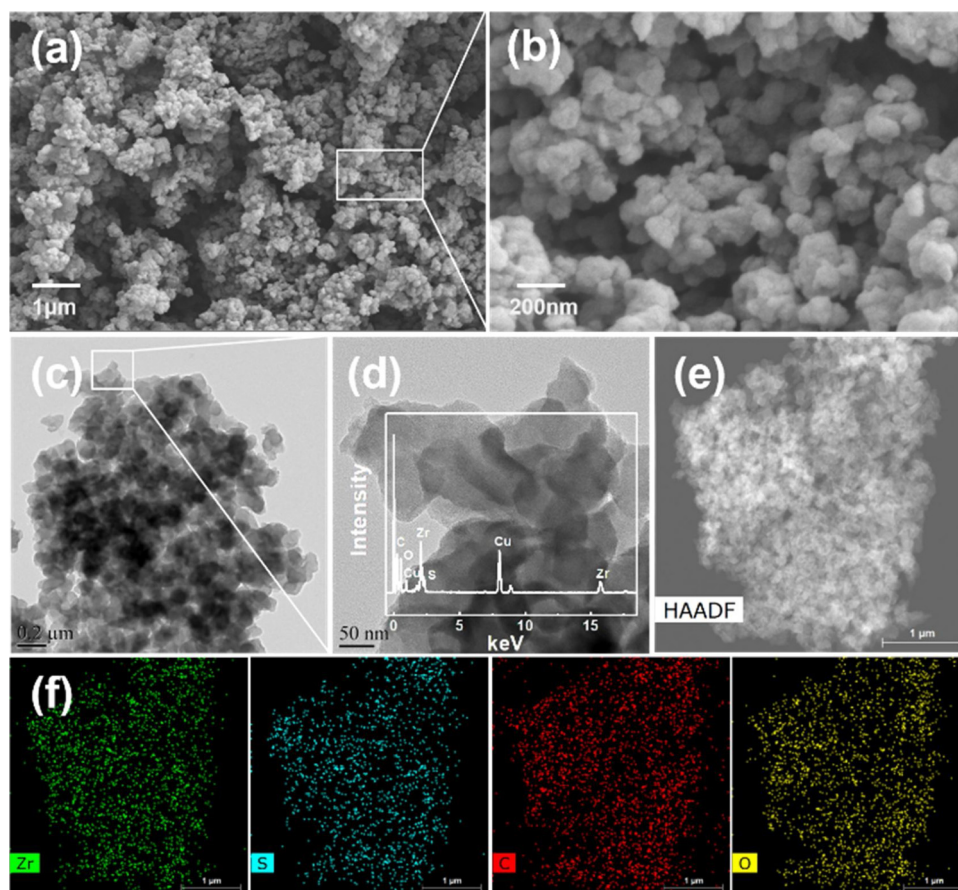


Fig. 1. SEM images (a, b) and TEM images (c, d) of Zr-LS; HAADF-STEM image (e) of Zr-LS and corresponding elemental mappings (f) of Zr, S, C and O.

active species. The X-ray diffraction pattern in Fig. 2b showed that Zr-LS exhibited a few broad diffractions without obvious crystallinity, further confirming the irregular connectivity between  $\text{Zr}^{4+}$  and LS and the amorphous structure of Zr-LS, which is unlike  $\text{ZrO}_2$  having high crystallinity with tetragonal (t) structure. As shown in the FT-IR spectra

(Fig. 2c), the enhanced transmittance at  $1116.7 \text{ cm}^{-1}$  and  $1039.6 \text{ cm}^{-1}$  were attributed to the anti-symmetry  $\text{SO}_2$  stretching vibration and  $\text{S}=\text{O}$  symmetric stretching vibration of sulfonic groups in LS chains, respectively. The samples also had a broad weak band at about  $655 \text{ cm}^{-1}$  and  $520 \text{ cm}^{-1}$ , which arose from  $-\text{C}-\text{S}$  bonds vibration of sulfonic

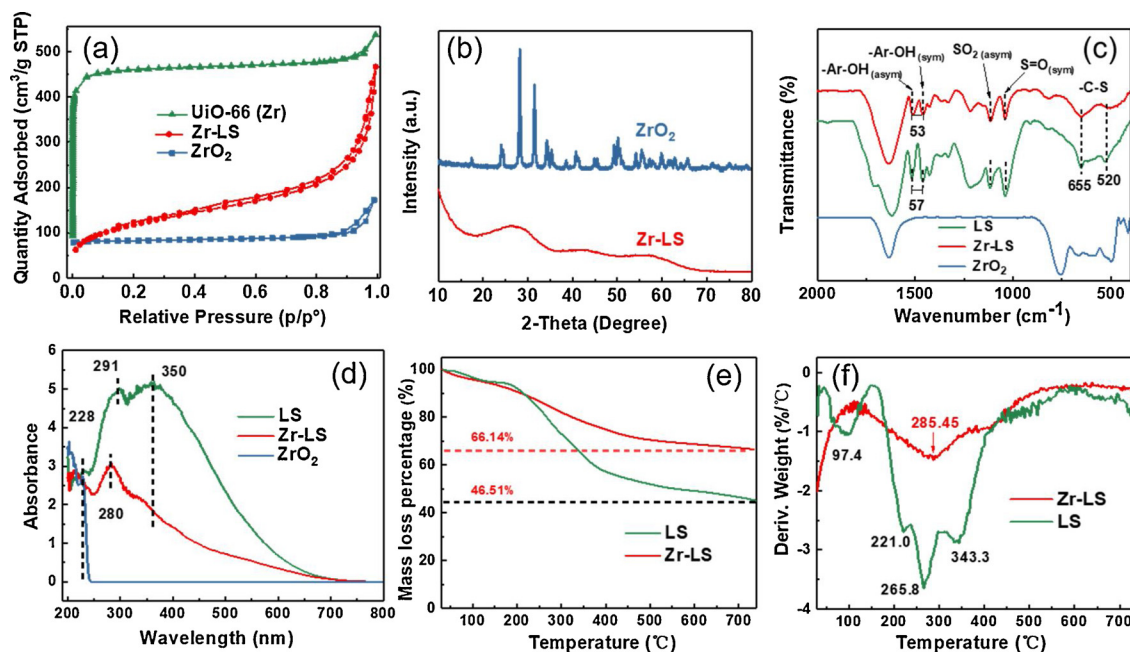


Fig. 2.  $\text{N}_2$  adsorption-desorption isotherm (a), XRD pattern (b), FT-IR spectra (c), UV-vis DRS spectra (d), TG (e) and DTG (f) curves of various catalysts.

groups, due to the presence of sodium sulfite or sodium bisulfite in sulfite pulping process. These FT-IR characteristic peaks indicated that the sulfonic groups remained after the hydrothermal preparation process. Meanwhile, the FT-IR spectrum of LS and Zr-LS displayed the characteristic anti-symmetry  $\text{-Ar-OH}$  stretching (LS,  $1517.4\text{ cm}^{-1}$ ; Zr-LS,  $1512.6\text{ cm}^{-1}$ ) and symmetric  $\text{-Ar-OH}$  stretching (LS,  $1460.5\text{ cm}^{-1}$ ; Zr-LS,  $1459.7\text{ cm}^{-1}$ ) of the phenolic hydroxyl group from the lignosulfonate chains [44]. These two different types of peaks were narrowed from  $57\text{ cm}^{-1}$  to  $53\text{ cm}^{-1}$  compared with the spectrum of LS, indicating that the phenolic hydroxyl groups of LS were coordinated to  $\text{Zr}^{4+}$  ions.

The coordination between LS and metal ion was also confirmed by UV-vis DRS (Fig. 2d). Evidently, the LS exhibited stronger absorption between 300–360 nm with a maximum at 350 nm. This electronic absorption band can be ascribed to non-conjugated phenolic groups in the lignosulfonate [45]. For Zr-LS, the  $\pi \rightarrow \pi^*$  absorption band was blue-shifted ( $\sim 280\text{ nm}$  from UV-vis DRS spectra), and had relatively weaker absorption in this area due to the metal chelation between large amount of phenolic hydroxyl groups on phenyl rings and  $\text{Zr}^{4+}$ . The UV-vis-DRS patterns of  $\text{ZrO}_2$  show an absorption band in the range of 205–230 nm which is attributed to the excitation of electron from valence band of  $\text{O}^{2-}$  (2p) to conduction band of  $\text{Zr}^{4+}$  (4d) [46].

TG and DTG analysis were conducted to study the thermal stability of Zr-LS and LS in the range of 50–750 °C (Fig. 2e, f). The weight loss of LS was clearly observed in four steps (97.4, 221.0, 265.8, 343.3 °C). These can be attributed to the loss of adsorbed water and the decomposition of organic species, indicating the instability of building block LS. Fig. 2f showed that the decomposition temperature of Zr-LS rose to 285.45 °C. The improvement of thermal stability further confirmed the coordination between LS and the  $\text{Zr}^{4+}$  ions.

We examined and compared the acid/base properties of Zr-LS,  $\text{ZrO}_2$  and other Zr-based MPV reduction catalysts (UiO-66, Zr-HAs, Zr-SBA-15) by  $\text{NH}_3$ -TPD and  $\text{CO}_2$ -TPD method (temperature-programmed desorption) (Fig. 3a, b). Larger amount of  $\text{NH}_3/\text{CO}_2$  desorbed and longer desorption time suggested that Zr-LS possessed higher contents of acid-base sites as compared with commercial  $\text{ZrO}_2$ . The results also indicated that more acid-base sites of as-prepared Zr-LS than other Zr-based MPV reduction catalysts (Table S2). This could be ascribed to the coordination between phenolic hydroxyl groups and  $\text{Zr}^{4+}$  promoting the formation of robust  $\text{-Ar-O-Zr-O-Ar-}$  frameworks that bore both

high content of acidic ( $\text{Zr}^{4+}$ ) and basic ( $\text{O}^{2-}$ ) sites during hydrothermal treatment of LS and  $\text{ZrCl}_4$ .

In order to have more insight into the Lewis and Brønsted acidic sites of catalyst, pyridine-adsorbed FT-IR spectra were conducted at two desorption temperatures of 110 °C and 250 °C under vacuum condition. As can be seen from Fig. 3c, five IR bands emerged at wavenumber of around 1450, 1490, 1550, 1610 and 1640  $\text{cm}^{-1}$  in Zr-LS. These bands were attributed to the pyridine interacting with Lewis acid sites (LA), or Brønsted acid sites (BA), or both of these two acid sites in Zr-LS [36]. The Lewis acid sites should originate from Zr centers and the Brønsted acid sites should originate from the  $\text{-SO}_3\text{H}$  in the molecular structure of LS. The forming reason of Brønsted acid sites ( $\text{-SO}_3\text{H}$ ) in Zr-LS is as follows: partial hydrolysis of  $\text{ZrCl}_4$  in the aqueous solution led to the formation of protonic acid (HCl). The occurrence of proton-exchange between  $\text{Na}^+$  and  $\text{H}^+$  impelled the formation of Brønsted acid sites ( $\text{-SO}_3\text{H}$ ). Trace Na element can be detected in Zr-LS, while 3.14% Na existed in LS through ICP-OES analysis further confirmed our speculation (Table S2). In addition, the quantitative analysis demonstrated that the amount of Lewis acid sites of Zr-LS was  $0.231\text{ mmol g}^{-1}$  at 110 °C and  $0.095\text{ mmol g}^{-1}$  at 250 °C, and the Brønsted acid sites of Zr-LS were  $0.079\text{ mmol g}^{-1}$  at 110 °C and  $0.031\text{ mmol g}^{-1}$  at 250 °C, respectively. These values were far stronger than that of  $\text{ZrO}_2$ . More and stronger acidity in Zr-LS was favorable for enhancing the adsorption of substrates and activating the carbonyl groups in aldehydes and hydroxyl groups in 2-PrOH, and thus promoted the MPV reduction reaction.

Apart from the content and nature of acid-base sites, the strength of active sites in different samples was examined by analyzing the local environment of Zr and O element through XPS technique. The survey spectra in Fig. 3d confirmed the presence of the Zr, O, C and S elements in Zr-LS. Zr 3d peaks showed that the binding energies at 180.03 eV and 182.40 eV which were assignable to Zr  $3d_{5/2}$  and  $3d_{3/2}$  shifted to a higher level (180.98 eV and 183.32 eV) in comparison with  $\text{ZrO}_2$  (Fig. 3e). This implied a higher positive charge on zirconium atoms in Zr-LS and thus manifested a stronger Lewis acidity of zirconium centers [24]. On the other hand, the binding energy of O1s belonging to  $\text{-Ar-O-Zr-O-Ar-}$  coordination interactions in Zr-LS was higher than for  $\text{-Zr-O-Zr-}$  interactions in  $\text{ZrO}_2$  and lower than  $\text{-Ar-OH}$  interactions in LS (Fig. 3f). The medium binding energy of O1s assigned to negative charge on the oxygen atoms manifested the medium basic

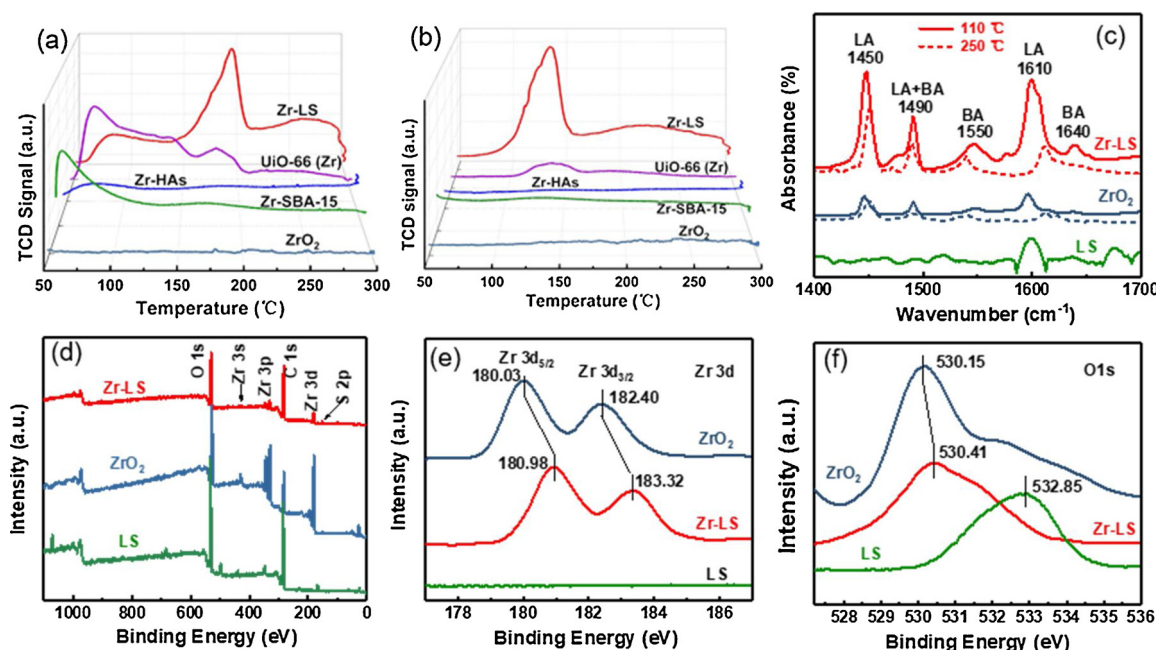


Fig. 3.  $\text{NH}_3$ -TPD (a),  $\text{CO}_2$ -TPD (b), Pyridine-adsorbed FT-IR spectra (c), XPS survey scan (d), Zr 3d XPS spectra (e) and O 1s XPS spectra (f) of various catalysts.

**Table 1**  
MPV reduction of FF to FA with various catalysts.<sup>a</sup>

Entry	Catalyst	T (°C)	Time (h)	Conv. (%)	FA yield (%)	FA selec. (%)	FDIA selec. (%) <sup>b</sup>	FA formation rate ( $\mu\text{mol g}^{-1} \text{h}^{-1}$ ) <sup>c</sup>	TOF ( $\text{h}^{-1}$ ) <sup>d</sup>	Carbon balance (%)
1	Blank	80	1	0	0	0	0	0	–	–
2	ZrO <sub>2</sub>	80	1	24.5	1.0	4.2	95.8	100	0.30	100
3	ZrSO <sub>4</sub>	80	1	26.2	0	0	96.9	0	0.75	97
4	ZrCl <sub>4</sub>	80	1	22.8	1.1	5.0	80.4	110	0.53	85
5	ZrOCl <sub>2</sub>	80	1	12.7	0.2	1.75	17.5	20	0.36	80
6	Zr(OH) <sub>4</sub>	80	1	35.2	34.5	97.9	2.1	3450	0.89	100
7	UiO-66 (Zr)	80	1	18.6	10.36	55.7	42.0	1036	0.53	98
8	LS	80	1	0.8	0	0	37.2	0	–	84
9	Zr–LS (0.5:1)	80	1	43.7	42.2	96.5	3.5	4217	1.98	100
10	Zr–LS	80	1	61.1	59.4	97.2	2.8	5940	2.74	100
11	Zr–LS (1.5:1)	80	1	62.1	60.9	98.1	1.9	6092	2.82	100
12	Zr–LS (2:1)	80	1	69.0	68.0	98.6	1.4	6803	3.13	100
13	Zr–LS	100	1	97.5	96.0	98.5	1.5	9600	4.37	100
14 <sup>e</sup>	ZrO <sub>2</sub>	140	2	89	60	67	–	7500	–	–
15 <sup>f</sup>	Zr-SBA-15	90	6	65.0	29.3	45.0	–	–	–	–
16 <sup>g</sup>	Zr-HAs	70	9	97.3	80.4	82.6	–	446.7	–	–
17 <sup>h</sup>	Zr–LS	100	1	26.2	16.8	64.3	17.7	1680	1.17	89
18 <sup>i</sup>	Zr–LS	100	1	86.0	85.4	99.3	0.7	8540	3.86	100
19 <sup>j</sup>	Zr–LS	100	1	92.2	91.6	99.4	0.3	9165	4.19	99

<sup>a</sup> Reaction conditions: 1 mmol FF in 10 ml 2-PrOH, 100 mg catalyst or 22% mol Zr.

<sup>b</sup> FDIA is furfural diisopropyl acetal (the acetalization product of FF with 2-PrOH).

<sup>c</sup> FA formation rate is defined as (mol of formed FA)/(catalyst amount  $\times$  time).

<sup>d</sup> TOF is defined as mol (converted FF)/[mol (total metal added)  $\times$  h (time)].

<sup>e</sup> Data obtained from Ref. [31].

<sup>f</sup> Data obtained from Ref. [42].

<sup>g</sup> Data obtained from Ref. [34].

<sup>h</sup> Base sites of Zr–LS were poisoned by adding 100 mg benzoic acid.

<sup>i</sup> Acid sites of Zr–LS were poisoned by adding 100 mg pyridine.

<sup>j</sup> Brønsted acid sites of Zr–LS were poisoned by adding 100 mg 2,6-lutidine.

strength of Zr–LS. In addition, a peak at 166.7 eV belonging to S 2p species in Zr–LS (Fig. S3), evidently indicated that sulfonic groups were preserved after hydrothermal process and these sulfonic groups in Zr–LS could facilitate the formation of Brønsted acidic sites [31]. These results showed the functional groups in LS could stabilize Lewis acidic Zr<sup>4+</sup> species and increase the basic contents achieved by the formation of porous –Ar–O–Zr–O–Ar– framework structure, although the Zr–O–Zr bonds in ZrO<sub>2</sub> seemed to give enhanced basic strength in comparison with Zr–LS.

### 3.2. Catalytic performance evaluation of the various catalysts

For our initial catalytic tests, we choose the MPV reduction of FF with 2-PrOH to examine the catalytic performance of different catalysts and the results were listed in Table 1. As anticipated, the blank run showed that the reduction reaction did not proceed without any catalyst at 80 °C for 1 h (Table 1, Entry 1). Then, different zirconium-containing compounds (ZrO<sub>2</sub>, ZrSO<sub>4</sub>, ZrCl<sub>4</sub>, ZrClO<sub>2</sub>, Zr(OH)<sub>4</sub>) were tested (Table 1, Entries 2–6). Neither Lewis acidic zirconium salts (ZrSO<sub>4</sub>, ZrCl<sub>4</sub> and ZrClO<sub>2</sub>) nor ZrO<sub>2</sub> with enhanced basic strength could efficiently catalyze MPV reduction of FF into FA and the furfural diisopropyl acetal (FDIA) derived from acetalization of FF with 2-PrOH was detected to be the dominant by-product (Fig. S6a). Moreover, UiO-66 (Zr), a conventional metal–organic framework, only gave a low FA yield of 10.36% (Table 1, Entry 7). In sharp contrast, Zr(OH)<sub>4</sub> showed relatively high catalytic activity with high FA selectivity (97.9%), moderate formation rate (3450  $\mu\text{mol g}^{-1} \text{h}^{-1}$ ) and TOF (0.89  $\text{h}^{-1}$ ). This result was consistent with literature results for effectively MPV reduction of 5-HMF and ethyl levulinate catalyzed by metal hydroxides bearing both acidic and basic sites [20,26,47]. Furthermore, the acidic LS precursor gave scarcely conversion of FF, suggesting that the building block for catalyst synthesis were not active in this reaction under the investigated conditions (Table 1, Entry 8). Gratifyingly, the prepared Zr–LS, which had both high strength acidic and basic sites, exhibited the highest conversion (61.1%), FA formation rate (5940  $\mu\text{mol g}^{-1} \text{h}^{-1}$ ) and TOF

(2.74  $\text{h}^{-1}$ ) with high selectivity (97.2%) at 80 °C for 1 h among these examined catalysts (Table 1, Entry 10). When the reaction temperature was further raised to 100 °C, a near quantitative yield (96.0%) and extremely high FA formation rate (9600  $\mu\text{mol g}^{-1} \text{h}^{-1}$ ) were obtained (Table 1, Entry 13). Moreover, the conversion of FF was remarkably increased from 43.7% to 61.1% as the initial ZrCl<sub>4</sub>/lignosulfonate mass ratios was increased from 0.5:1 to 1:1 (Table 1, Entries 9–12). However, further elevating ZrCl<sub>4</sub>-initial loading amounts has only slightly improved the FF conversion. This is due to the amount of phenolic hydroxyl groups in sodium lignosulfonate is constant. Lignosulfonate could only coordinate with a certain amount of Zr<sup>4+</sup>. In addition, the prepared Zr–LS had better catalytic activity than other Zr-containing catalysts reported in the recent literature (Zr-HAs, Zr-SBA-15, ZrO<sub>2</sub>) under comparable or more harsh reaction conditions (Table 1, Entries 14–16). As we discussed above, the contents of the acidic and basic sites of Zr–LS were more than ZrO<sub>2</sub> and other Zr-based MPV reduction catalysts (UiO-66, Zr-HAs, Zr-SBA-15) by analyzing the results of NH<sub>3</sub>-TPD and CO<sub>2</sub>-TPD. Therefore, we speculate that the presence of both acidic and basic sites with appropriate content and strength in the prepared catalytic materials seemed to be key factors for the selective reduction of FF into FA combining with characterizations of catalysts and the above experimental results. In order to confirm our speculation and obtain more insight toward the role of acid-base active sites in Zr–LS on MPV reduction, pyridine, 2,6-lutidine and benzoic acid as poisoning additives were separately introduced into the reaction system. In the presence of benzoic acid, a drastically drop of FF conversion and FA selectivity was observed, indicating that the Zr–LS catalyzed MPV reduction was closely related to basic sites on the catalyst surface (Table 1, Entry 17). Further, the addition of pyridine also reduced the conversion of FF (Table 1, Entry 18). When the Brønsted acid were selectively poisoned by adding 2,6-lutidine, the catalytic activity of Zr–LS was also slightly decreased, indicating that the presence of Brønsted acid in Zr–LS can be helpful for MPV reduction of FF (Table 1, Entry 19). By consulting relevant literatures, we know that the poisoning effect of pyridine or 2,6-lutidine is weak when compared with benzoic acid [48]. Therefore,

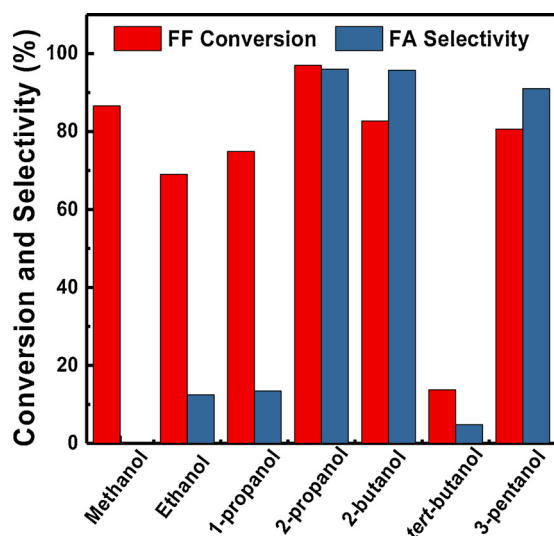


Fig. 4. Influence of hydrogen donor on MPV reduction of FF catalyzed by Zr-LS. Reaction conditions: 1 mmol FF in 10 ml solvent, 100 mg catalyst, 100 °C, 1 h.

the addition of pyridine or 2,6-lutidine only slightly reduced the conversion of FF due to partial poisoning of acidic sites. These poisoning tests further verified both of acid-base sites are essential for the high catalytic performance of Zr-LS in MPV reduction of FF.

### 3.3. Influence of hydrogen donor

The influence of the hydrogen donor on the MPV reduction of FF catalyzed by Zr-LS was investigated and the results are depicted in Fig. 4. When primary alcohols (methanol, ethanol and 1-propanol) were used, the acetalization reaction proceeded faster than MPV reduction. A large number of bulky by-products such as furfural dimethyl acetal and furfural diethyl acetal and were obtained in yield of 86.5% and 60.4%, respectively. When *tert*-butanol was selected as solvent and hydrogen source, we get extremely low conversion of FF, suggesting that the presence of  $\beta$ -H in alcohol is essential for MPV reduction reaction. Therefore, primary alcohols and tertiary alcohol did not work as hydrogen donors. In contrast, satisfactory FF conversion and FA selectivity were obtained when some secondary alcohols such as 2-PrOH, 2-butanol and 3-pentanol were employed as H-donor. Moreover, with the increase of carbon number in secondary alcohol, the conversion of FF decreased a little. The possible reason for this phenomenon is that longer carbon chains of the secondary alcohol could lead to more significant negative steric effect, which hinders the diffusion of substrate molecules into channels of Zr-LS. Therefore, 2-propanol was the best H-donor and solvent for MPV reduction of aldehydes over Zr-LS.

### 3.4. The reaction kinetics study

To further reveal the relationship between acid-base catalytic active sites of the as-prepared Zr-LS catalyst and their catalytic performance, reaction kinetic experiment was conducted. In order to determine the kinetic data more accurately and avoid mass transfer limitations, the experiment for FF reduction was performed under low reaction temperature (100 °C) with 30, 65 and 100 mg catalysts (Fig. 5a). It can be observed that the FF conversion increased rapidly with an increase in Zr-LS amount. FF conversion can reach 100% by prolonging the reaction time to 2 h with 100 mg catalyst. Meanwhile, the selectivity toward FA also increased from 81% to 96% with the increase of Zr-LS amount, indicating more acid-base sites can promote the equilibrium shift from the acetalization reaction toward MPV reduction reaction. The effect of the number of bifunctional acid-base sites of Zr-LS on the

FF conversion rate was depicted in Fig. 5b. The concentration of acid-base sites was obtained from  $\text{NH}_3$ -TPD and  $\text{CO}_2$ -TPD tests (Table S2). The reaction rate was measured by collecting FF conversion data at 30 min. We can observe that a linear relationship between the reaction rate of FF and the concentration of acid-base sites in Zr-LS. This signified that the FF conversion rate had a first-order dependence on the concentration of acid-base sites, supporting that the adsorption and activation of substrate molecule on acid-base sites in Zr-LS was the rate-determining step.

The effect of the concentration of 2-PrOH on MPV reduction of FF was investigated. The volume of 2-PrOH was changed in the range from 2.5 ml to 10 ml and toluene was added to keep the volume of solvent constant. Fig. 5c showed the effect of concentration of 2-PrOH on MPV reduction of FF to FA at 100 °C. When the concentration of 2-PrOH was only 25%, the FF conversion increased extremely slowly with prolongation of reaction time. With the elevated concentration of 2-PrOH from 25% to 100%, the FF conversion increased more rapidly and 99% conversion was obtained after reaction at 100 °C for 2 h. This result indicated that the concentration of 2-PrOH as both hydrogen donor and solvent is also key factor for the reductive transformation of FF.

The effect of concentration of 2-PrOH on the MPV reduction rate was shown in Fig. 5d. TOF value was regarded as the reaction rate, which was calculated according to the conversion of FF within 30 min from Fig. 5c. It's obvious that the reaction rate of FF also followed a first-order dependence on the concentration of 2-PrOH. The first-order dependence of the hydrogen donor supported a reaction mechanism in which the direct hydride transfer on catalytic active sites was involved in the rate-limiting step. Further information about the catalytic reaction mechanism in Zr-LS will be illustrated in the part of Reaction mechanism studies.

The effect of the reaction temperature on FF conversion over Zr-LS was also studied. As depicted in Fig. 6a and b, the reaction temperature demonstrated a remarkable effect on the catalytic performance of Zr-LS for the MPV reduction of FF from 60 to 80 °C. When the reaction was performed at low reaction temperature (60 °C) for 40 min, both low conversion (27.1%) of FF and selectivity (75.2%) of FA was obtained. The conversion of FF dramatically increased to 77.0% and the FA selectivity also increased significantly to a higher value of 86.0% as the reaction temperature was increased to 100 °C. Additionally, the FF conversion can reach 99.0% with high FA selectivity (96.0%) by prolonging reaction time to 2 h at 100 °C. Meanwhile, the acetalization products (furfural diisopropyl acetal) of FF with 2-PrOH gradually decreased with the raised reaction temperature from 60 °C to 100 °C (Fig. 6b), indicating that the equilibrium shift from the acetalization reaction to MPV reduction can be enhanced by elevating the reaction temperatures. However, the selectivity of FA gradually declined due to etherification of FA with 2-PrOH to 2-(isopropoxy)methyl furan with further increased reaction temperature (120 °C). Therefore, the suitable temperature was 100 °C for preparing FA with high selectivity.

Since the content of catalyst was fixed and hydrogen donor was in great excess, we hypothesize that the reaction was a first-order reaction as a function of FF concentration. It's obvious that  $\ln(c_0/c_t)$  followed a linear relationship with reaction time  $t$  at FF low conversion (Fig. 6c). By calculating the corresponding slope of the plots, the reaction rate constants ( $k$ ) were calculated to be 0.00407, 0.00992, 0.03226  $\text{min}^{-1}$  for the reaction temperatures of 60, 80 and 100 °C, respectively. On the basis of the Arrhenius plot in Fig. 6d, the apparent activation energy ( $E_a$ ) was determined to be 52.25  $\text{kJ mol}^{-1}$  over the Zr-LS catalyst for the MPV reduction of FF into FA. This  $E_a$  value was lower than our previous  $E_a$  value (83  $\text{kJ/mol}$ ) of Mn-NCA-700 for the same reaction and comparable to those of latest reported heterogeneous catalysts for the production of FA from FF (Table S3). We have also compared our developed Zr-LS catalyst for the selective reduction of FF with other earlier reported literatures which were summarized in Table S3. Obviously, Zr-LS can produce nearly quantitative FA yield (96.0%) under more mild conditions (80–120 °C).

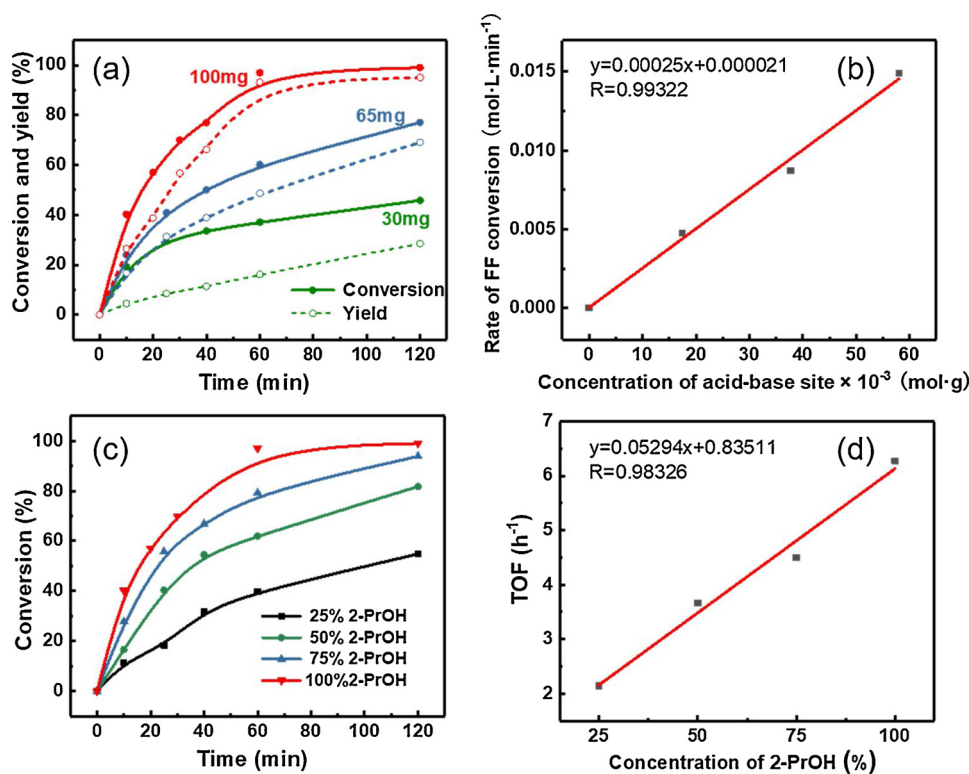


Fig. 5. Effect of Zr-LS amount on MPV reduction of FF to FA (a). Effect of the concentration of acid-base sites on FF conversion rate at a reaction time within 30 min (b). Effect of concentration of 2-PrOH on MPV reduction of FF to FA (c). TOF values for conversion of FF with different 2-PrOH concentrations at a reaction time within 30 min (d).

There were mainly three reasons accounting for the excellent catalytic performance of Zr-LS with high selectivity: (1) Poisoning experiments authenticated that the catalyst with high content of basic sites was crucial to improve the catalytic activity for MPV reduction. A large number of phenolic hydroxyl groups in the chains of lignosulfonate can provide abundant and strong basic sites ( $O^{2-}$ ) in

coupled  $Zr^{4+}-O^{2-}$  species after coordinating with  $Zr^{4+}$ , thus significantly enhancing the conversion rate. (2) Poisoning experiments also indicated that the Lewis acidic sites play an important role in selective reduction of FF into FA. After hydrothermal self-assembly between strong Lewis acid  $ZrCl_4$  and lignosulfonate, Zr-LS can still retain Lewis acidity with appropriate content and strength. This is another key

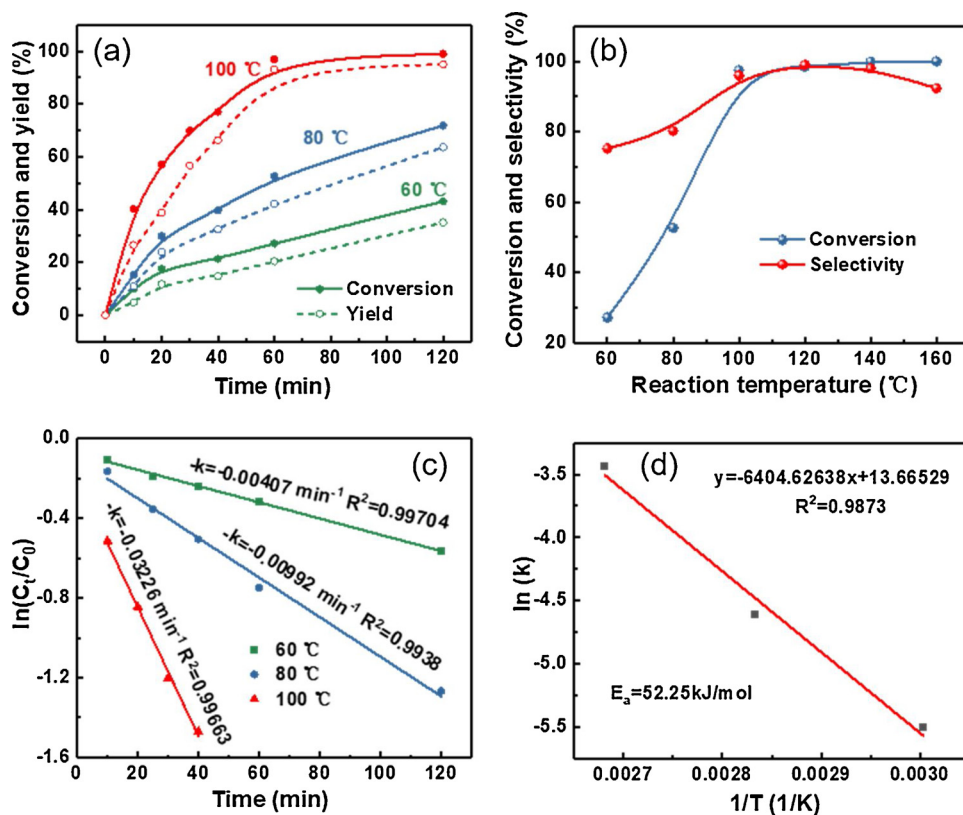


Fig. 6. Effect of reaction temperature on MPV reduction of FF to FA (a). Effect of reaction temperature of FF conversion and FA selectivity, Reaction time: 1 h (b). First-order kinetic fit for MPV reduction of FF to FA at different temperatures (c). The corresponding Arrhenius plots for Zr-LS (d). Reaction conditions: 1 mmol FF in 10 ml 2-PrOH, 100 mg Zr-LS catalyst.

factor for highly selective reduction of FF into FA because stronger Lewis acidity could promote undesirable side reactions. (3) Previous studies had demonstrated that the Brønsted acidic  $-\text{SO}_3\text{H}$  groups could also activate the carbonyl group [14,49]. Thus, the inherent sulphonic groups from lignosulfonate chains in Zr-LS were the other catalytic active sites contributing to enhanced performance in the MPV reduction reaction of FF. Moreover, it is worth mentioning that the raw material for catalyst synthesis is lignosulfonate, a waste by-product of the paper industry. From the viewpoint of the reaction conditions and the cost for catalyst preparation, the Zr-LS catalyst had obvious advantages and showed a greater potential in the practical application.

### 3.5. MPV reduction of other carbonyl compounds

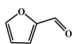
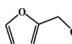
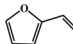
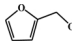
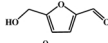
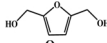
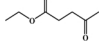
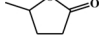
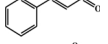
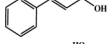
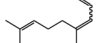
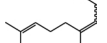
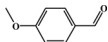
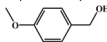
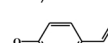
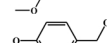
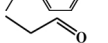
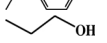
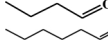
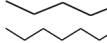
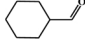
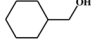
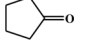
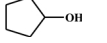
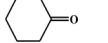
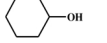
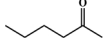
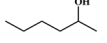
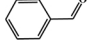
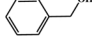
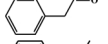
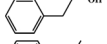
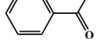
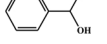
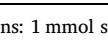
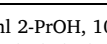
Besides the high activity of Zr-LS in catalytic transformation of FF, the highly efficient MPV reduction of other biomass-based platform compounds is also of great significance. Accordingly, the general scope of the prepared Zr-LS was investigated. 5-hydroxymethylfurfural (5-HMF), which can be obtained from C6 carbohydrates, is also considered as a versatile platform chemical [50–52]. Clearly, the developed Zr-LS exhibited also superior high activity toward 5-HMF and more than 98% conversion with 91% selectivity to the corresponding alcohol was obtained (Table 2, Entry 3). The only by-product of this reaction was 5-(isopropylmethyl) furfuryl alcohol (the etherification product of reduced alcohol with 2-PrOH) based on the results of GC-MS. This etherification product was also particularly important and could serve as a promising fuel additive owing to their high energy density [53,54]. Another lignocellulose-derivative ethyl levulinate was also efficiently converted into  $\gamma$ -valerolactone with a high selectivity of 91% at 150 °C

within 8 h (Table 2, Entry 4). Furthermore, other biomass-based carbonyl compounds were also used as substrates to investigate the feasibility of Zr-LS. For example, cinnamaldehyde, citral and veratraldehyde could be successfully reduced into corresponding alcohols with both high conversion (> 90%) and selectivity (> 90%) (Table 2, Entries 5–7). These corresponding alcohols are important organic intermediates with wide applications in manufacturing pharmaceuticals, flavors and cosmetics, etc. Besides the reduction of bioderived platform molecules, other typical aldehydes and ketones from traditional chemical industry were also tested as substrates to examine the catalytic potential of Zr-LS (Table 2, Entries 8–18). In these reactions, high conversions (90–99%) of all substrates with excellent selectivities (91 to 100%) were produced. However, the MPV reductions of ketones with electron-donating alkyl groups were more difficult. For example, higher reaction temperature (150 °C) and longer reaction time (8 h) were needed for 1-phenylethanol to obtain satisfactory yields of acetophenone (Table 2, Entry 18). The wide substrate scope indicates that the Zr-LS catalyst was a highly versatile catalyst for MPV reduction of both biomass-based platform compounds and other commercial aldehydes to alcohols.

### 3.6. Time course of the MPV reduction of FF over Zr-LS

In order to investigate the reaction pathway, the time course of MPV reduction of FF over the Zr-LS catalyst was recorded at 100 °C. Fig. 7 recorded the products distribution during the reaction process of the MPV reduction of FF with 2-propanol. It was observed that FF was completely consumed and FA was produced in a yield of 96% at 100 °C after 2 h. Besides the formation of FA, FDIA (furfural diisopropyl acetal, the acetalization of FF with 2-PrOH) was observed to be the only by-

**Table 2**  
Results of Zr-LS-catalyzed MPV reduction of various carbonyl compounds to alcohols.<sup>a</sup>

Entry	Substrates	Products	Time (h)	T (°C)	Conv. (%)	Selec. (%)
1			3	80	97	97
2			1	100	98	99
3 <sup>b</sup>			2	100	98	91
4			8	150	90	91
5			3	80	95	98
6			14	100	98	100
7			4.3	80	90	99
8			4	80	93	99
9			1.2	80	92	98
10			1.5	80	98	94
11			1.7	80	93	91
12			1.7	80	95	94
13			4	80	90	100
14			5	80	96	100
15			8	150	91	99
16			2	80	99	99
17			2	80	91	96
18			8	150	93	95

<sup>a</sup> Reaction conditions: 1 mmol substrates in 10 ml 2-PrOH, 100 mg catalyst.

<sup>b</sup> The by-product is 5-(isopropylmethyl) furfuryl alcohol (the etherification product of 2,5-bis-(hydroxymethyl)-furan with 2-PrOH).

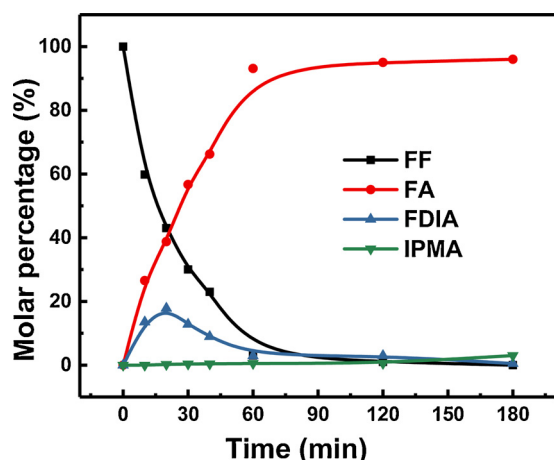


Fig. 7. The products distribution during the MPV reduction of FF with 2-PrOH to FA. Reaction conditions: 1 mmol FF in 10 ml 2-PrOH, 100 mg Zr–LS catalyst, 100 °C.

product especially in a short reaction time. It was interesting to note that FDIA was not stable and could be reversibly converted to FF with the increase of the reaction time. Nevertheless, etherification reaction of the generated FA with 2-PrOH didn't happened at the initial stage. After extending the reaction time to 3 h, the FA yield decreased slightly and 2-(isopropoxymethyl)furan (IPMA) as side products was formed and increased (Fig. S6b). This result suggested that the Brønsted acidic active sites in Zr–LS can also catalyze the etherification reaction of the generated FA with 2-PrOH (Scheme S1) when the MPV reduction of FF was completed. This reaction is also particularly important for the upgradation of biomass because ethers of furfural/5-hydroxymethyl furfural and its derivatives hold particular promise as fuel additives. Further studies on how to increase the Brønsted acidic sites in Zr–LS and one-step reductive etherification of furfural/5-hydroxymethyl furfural are now in progress.

### 3.7. Heterogeneity and recycling experiments

In order to prove that the catalyst is heterogeneous, we filtered the Zr–LS catalyst from the solvent after 20 min at 100 °C. Afterwards, the FF reduction reaction was allowed to react for another 160 min under identical conditions without Zr–LS catalyst (Fig. 8a). It can be observed that the FF conversion was still maintained at 56.5%. ICP-OES result also showed that there was no apparent compositional change in the filtered sample, implying that no active species were leached into the reaction mixture and the heterogeneous character of Zr–LS. Furthermore, the recycling experiments of Zr–LS for MPV reduction of FF was investigated by keeping approximately 60% FF conversion at 80 °C for

1 h (Fig. 8b). FF conversion was only slightly reduced from 61% to 58% in seven consecutive reaction cycles and the selectivity of FA remained unchanged in all runs. The recycled Zr–LS in the seventh run was characterized by SEM, XRD, XPS, FT-IR and pyridine-adsorbed FT-IR. SEM showed that the average diameter of recovered Zr–LS catalyst was slightly decreased from 148.9 nm to 134.7 nm due to the magnetic stir in seven consecutive reaction cycles (Fig. S4a–d). XRD patterns and FT-IR proved that the amorphous morphology and microstructures of the recovered Zr–LS remained largely unchanged as compared to that of the fresh catalyst (Fig. S5a, d). In addition, XPS and the pyridine-adsorbed FT-IR spectra indicated that there was no significant change in the strength and amount of acidity and basicity, and the distribution of Lewis acid and Brønsted acid sites before and after seven cycles of reactions (Fig. S5b, c, e). ICP-OES analyses showed that less than 2.6 and 6.4 ppm of Zr and S species were leached into the filtrate after the seventh round of reactions. This result suggested the loss of a small amount of Zr active sites during process of seven recycling, thus contributing to the slightly decrease of catalytic performance.

### 3.8. Reaction mechanism studies

To elucidate the FF reduction mechanism by Zr–LS, isotopic labeling experiment in different deuterated 2-PrOH was conducted (Fig. S4). The GC–MS fragmentation showed that the parent ion of the FA in unlabeled 2-PrOH is the same as the FA standard (Fig. 9a). However, this parent ion increased to 99 when 2-PrOH was labeled (2-PrOH-d8), indicating that one H atom in FA product was replaced by a deuterium (D) atom. To clarify whether the reaction proceeded via direct hydrogen transfer or metal dihydride route (Scheme S2), 2-PrOH-OD was used as H-donor for FF reduction. The mass fragmentation showed that the parent ion of FA product in labeled 2-PrOH-OD was also  $m/z = 98$ , which is closely similar to that in 2-PrOH. In addition, the  $m/z$  shift equaled to 1 when 2-PrOH-OD and 2-PrOH-d8 were respectively used as hydrogen source (Scheme S3 and S4). These results suggested that there was no H scrambling between O of 2-PrOH and  $\alpha$ -C of FF, thus explicitly substantiating that Zr–LS facilitate the reduction of FF through direct hydrogen transfer [55]. It is worth noting that in both hydrogenation mechanisms (Scheme S2), the FA molecule contains two Ds using 2-propanol-d8. The discrepancy between the predicted and observed mass shifts (2 and 1 amu, respectively) can be rationalized by the fact that the deuterium in the OD group of FA can exchange the OH groups in the capillary gas chromatograph (GC) column [55].

We also perform ex situ  $^1\text{H}$  NMR spectra to further prove this mechanism by demonstrating the location of the replaced deuterium (Fig. 9b). It was observed that all samples in 2-PrOH or deuterated 2-PrOH exhibited 4 distinct peaks of FA at 7.33 ppm, 6.24 ppm, 6.18 ppm and 4.39 ppm. The front three peaks were characteristic peak of H atoms on the furan ring. The last peak ( $\text{H}_d$ ) can be attributed to the hydrogen atom at  $\alpha$ -C. The ratio of peak height ( $\text{H}_d:\text{H}_c$ ) can

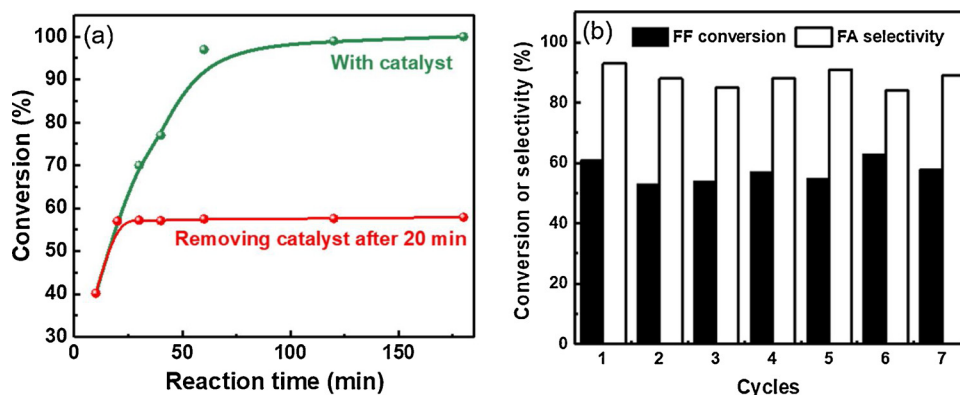


Fig. 8. Heterogeneity (a) and reusability (b) of the Zr–LS catalyst in MPV reduction of FF.

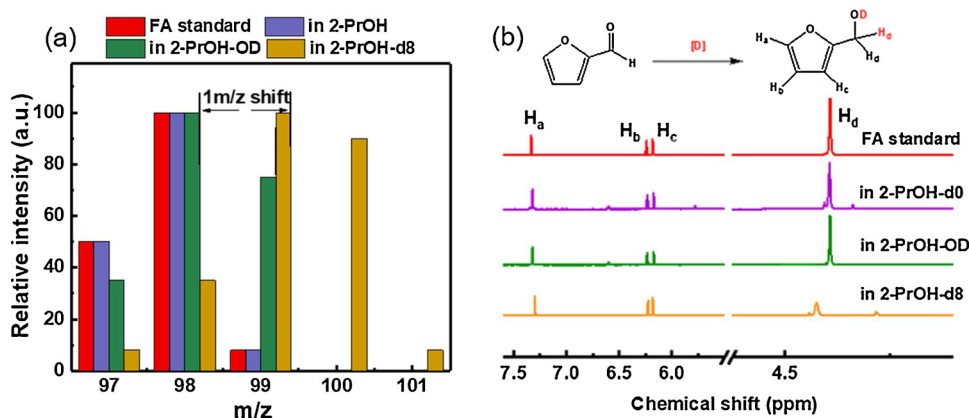


Fig. 9. GC-MS spectra (a) and  $^1\text{H}$  NMR spectra (b) of FA standard and FA product in different solvents.

approximately represent the relative number of H at different locations. It was observed that  $\text{H}_d:\text{H}_c$  in FA standard sample, and FA synthesized in 2-PrOH and 2-PrOH-OD is around 2:1. However, slight chemical shift of  $\text{H}_d$  between FA formed in 2-PrOH-d8 and normal FA occurred. Meanwhile, the ratio of peak height ( $\text{H}_d:\text{H}_c$ ) decreased to 1:1, implying that one hydrogen atoms at the  $\alpha$ -C was replaced by deuterium atom. Furtherly, the reaction rate for the reduction of FF in normal ( $k_H$ ) 2-PrOH and isotopic ( $k_D$ ) 2-PrOH was determined respectively under the same conditions. In the case of 2-PrOH-OD, no KIE (intermolecular kinetic isotope effect) was observed ( $k_H/k_D = 1.16$ ). In contrast, a larger KIE of 2.286 was observed when 2-PrOH-d8 was used as hydrogen source. The different kinetic isotope effect further corroborate that the reaction involves the cleavage of  $\beta$ -H in 2-PrOH and this direct hydride transfer step between aldehyde and alcohol was the rate-determining step for MPV reduction.

As discussed above, the Lewis acid-base couple sites and Brønsted acid sites were crucial for the MPV reaction of carbonyl compounds to alcohols. In combination with the results of physicochemical characterizations, catalytic performance evaluation, poisoning experiments, dynamics experiment, isotopic tracing experiments and previous reports, we proposed a plausible reaction mechanism for Zr-LS catalyzed reduction of carbonyl compounds (Scheme 2). In the first step, 2-PrOH was adsorbed on Zr-LS, resulting in its dissociation to alkoxide and

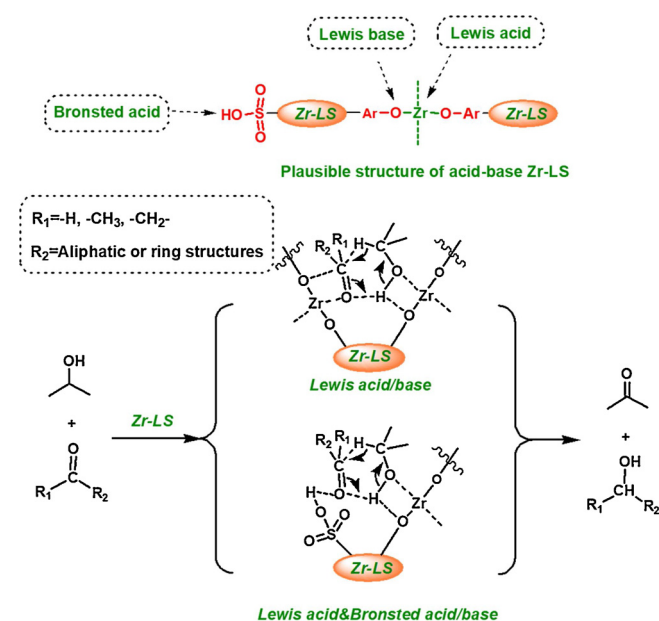
hydrogen by the acid–basic coupled sites ( $\text{Zr}^{4+}-\text{O}^{2-}$ ). Meanwhile, the deprotonation of 2-PrOH was enhanced by the basic phenate  $\text{O}^{2-}$  atoms [24]. The carbonyl group in the substrate molecules was activated by Lewis acidic  $\text{Zr}^{4+}$  species or electron-withdrawing Brønsted acid sites (sulfonic groups) [49,56]. Next, the six-membered ring transition state was formed with carbonyl groups and 2-PrOH, leading to direct hydride transfer via  $\beta$ -H elimination and yielding corresponding alcohols and acetone.

#### 4. Conclusions

In summary, we have constructed a Zr-containing catalyst, using lignosulfonate, a by-product from sulphite pulping process, as the building block. The resulting Zr-LS possessed high activity in the MPV reduction of biomass-derived oxygenates, especially for the reduction of FF to FA in quantitative yields (96%) under mild conditions (80 °C within 3 h). Compared with previous reports, our prepared Zr-LS has three significant advantages: i) From waste to wealth: the raw material lignosulfonate is renewable, low-cost and abundant, ii) The fabrication process only involves a facile, nontoxic and scalable hydrothermal synthesis, and iii) the inherent sulfonic groups in lignosulfonate could serve as Brønsted acidic sites avoiding the use of hazardous sulfonating agents. Kinetic studies revealed that  $E_a$  of the MPV reduction of FF was estimated to be 52.25 kJ/mol. Mechanism studies indicated that the cooperative role of strong Lewis acid-base couple sites ( $\text{Zr}^{4+}-\text{O}^{2-}$ ) and moderate Brønsted acidic sites ( $-\text{SO}_3\text{H}$ ) in Zr-LS contributed to the outstanding catalytic performance in MPV reduction. Isotopic labeling experiments demonstrated direct hydrogen transfer from  $\alpha$ -C of 2-PrOH to the  $\alpha$ -C of FF based on the formation of six-membered intermediates was the rate-determining step. Furtherly, the Zr-LS could be reused at least seven consecutive cycles with no distinct changes in activity and structures. The utilization of lignocellulosic derivatives as feedstocks for both fabricating highly active biomacromolecule catalysts and producing valuable platform chemicals in this study presents a sustainable chemical conversion process.

#### Acknowledgements

The authors thank the financial support for this work by the National Natural Science Foundation of China (21774036), the Recruitment Program of Global Youth Experts, the State Key Laboratory of Pulp and Paper Engineering (No. 2017TS01), Guangdong Province Science Foundation (2017B090903003, 2017GC010429, 201704030066), the Guangdong Province Youth Science and Technology Innovation Talents (Grant No. 2014TQ01C781) and the Science and Technology Planning Project of Guangdong Province, China (Grant No. 2016B090918074).



Scheme 2. Plausible structure of acid–base Zr-LS and possible mechanism for the Zr-LS-catalyzed MPV reactions of carbonyl compounds.

## Appendix A. Supplementary data

Supplementary material related to this article can be found, in the online version, at doi:<https://doi.org/10.1016/j.apcatb.2019.02.011>.

## References

- [1] E.L. Kunkes, D.A. Simonetti, R.M. West, J.C. Serrano-Ruiz, C.A. Gärtner, J.A. Dumesic, Catalytic conversion of biomass to monofunctional hydrocarbons and targeted liquid-fuel classes, *Science* 322 (2008) 417–421.
- [2] D.M. Alonso, S.G. Wettstein, M.A. Mellmer, E.I. Gurbuz, J.A. Dumesic, Integrated conversion of hemicellulose and cellulose from lignocellulosic biomass, *Energy Environ. Sci.* 6 (2012) 76–80.
- [3] H.P. Winoto, Z.A. Fikri, J.M. Ha, Y.K. Park, H. Li, D.J. Suh, J. Jae, Heteropolyacid supported on Zr-beta zeolite as an active catalyst for one-pot transformation of furfural to  $\gamma$ -valerolactone, *Appl. Catal. B: Environ.* 241 (2019) 588–597.
- [4] C. Li, X. Zhao, A. Wang, G.W. Huber, T. Zhang, Catalytic transformation of lignin for the production of chemicals and fuels, *Chem. Rev.* 115 (2015) 11559–11624.
- [5] A.J. Ragauskas, G.T. Beckham, M.J. Biddy, R. Chandra, F. Chen, M.F. Davis, B.H. Davison, R.A. Dixon, P. Gilna, M. Keller, Lignin valorization: improving lignin processing in the biorefinery, *Science* 344 (2014) 1246843.
- [6] M.M. Antunes, S. Lima, A. Fernandes, M.F. Ribeiro, D. Chadwick, K. Hellgardt, M. Pillinger, A.A. Valente, One-pot hydrogen production and cascade reaction of furfural to bioproducts over bimetallic Pd-Ni TUD-1 type mesoporous catalysts, *Appl. Catal. B: Environ.* 237 (2018) 521–537.
- [7] R.J. Chimentão, H. Oliva, J. Belmar, K. Morales, P. Mäki-Arvel, J. Wärnå, D.Yu. Murzin, J.L.G. Fierro, J. Llorca, D. Ruiz, Selective hydrodeoxygenation of biomass derived 5-hydroxymethylfurfural over silica supported iridium catalysts, *Appl. Catal. B: Environ.* 241 (2019) 270–283.
- [8] J.Q. Bond, D.M. Alonso, D. Wang, R.M. West, J.A. Dumesic, Integrated catalytic conversion of gamma-valerolactone to liquid alkenes for transportation fuels, *Science* 327 (2010) 1110–1114.
- [9] R.F. Perez, O.S.G.P. Soares, A.M.D. de Farias, M.F.R. Pereira, M.A. Fraga, Conversion of hemicellulose-derived pentoses over noble metal supported on 1D multiwalled carbon nanotubes, *Appl. Catal. B: Environ.* 232 (2018) 101–107.
- [10] S. Zhou, G. Chen, X. Feng, M. Wang, D. Liu, F. Lu, H. Qi, In situ  $\text{MnO}_x/\text{N}$ -doped carbon aerogels from cellulose as monolithic and highly efficient catalysts for the upgrading of bioderived aldehydes, *Green Chem.* 20 (2018) 3593–3603.
- [11] L. Jiang, L. Zhou, J. Chao, H. Zhao, T. Lu, Y. Su, X. Yang, J. Xu, Direct catalytic conversion of carbohydrates to methyl levulinate: synergy of solid Brønsted acid and Lewis acid, *Appl. Catal. B: Environ.* 220 (2017) 589–596.
- [12] H. Li, Z. Fang, J. Luo, S. Yang, Direct conversion of biomass components to the biofuel methyl levulinate catalyzed by acid-base bifunctional zirconia-zeolites, *Appl. Catal. B: Environ.* 200 (2017) 182–191.
- [13] Z. Yuan, L. Wang, J. Wang, S. Xia, P. Chen, Z. Hou, X. Zheng, Hydrogenolysis of glycerol over homogeneously dispersed copper on solid base catalysts, *Appl. Catal. B: Environ.* 101 (2011) 431–440.
- [14] L. Bui, H. Luo, W.R. Gunther, Y. Román-Leshkov, Domino reaction catalyzed by zeolites with Brønsted and Lewis acid sites for the production of  $\gamma$ -valerolactone from furfural, *Angew. Chem. Int. Ed.* 52 (2013) 8022–8025.
- [15] R. Mariscal, P. Maireles-Torres, M. Ojeda, I. Sádaba, M.L. Granados, Furfural: a renewable and versatile platform molecule for the synthesis of chemicals and fuels, *Energy Environ. Sci.* 9 (2016) 1144–1189.
- [16] R.-J. van Putten, J.C. Van Der Waal, E. De Jong, C.B. Rasrendra, H.J. Heeres, J.G. de Vries, Hydroxymethylfurfural, a versatile platform chemical made from renewable resources, *Chem. Rev.* 113 (2013) 1499–1597.
- [17] Y. Yan, K. Li, J. Zhao, W. Cai, Y. Yang, J. Lee, Nanobelt-arrayed vanadium oxide hierarchical microspheres as catalysts for selective oxidation of 5-hydroxymethylfurfural toward 2, 5-diformylfuran, *Appl. Catal. B: Environ.* 207 (2017) 358–365.
- [18] G.-H. Wang, J. Hilgert, F.H. Richter, F. Wang, H.-J. Bongard, B. Spliethoff, C. Weidenthaler, F. Schüth, Platinum-cobalt bimetallic nanoparticles in hollow carbon nanospheres for hydrogenolysis of 5-hydroxymethylfurfural, *Nat. Mater.* 13 (2014) 293–300.
- [19] L.S. Ribeiro, J.J. Delgado, J.J.M. Órfão, M.F.R. Pereira, Carbon supported Ru-Ni bimetallic catalysts for the enhanced one-pot conversion of cellulose to sorbitol, *Appl. Catal. B: Environ.* 217 (2017) 265–274.
- [20] W. Hao, W. Li, X. Tang, X. Zeng, Y. Sun, S. Liu, L. Lin, Catalytic transfer hydrogenation of biomass-derived 5-hydroxymethyl furfural to the building block 2,5-bis(hydroxymethyl) furan, *Green Chem.* 18 (2016) 1080–1088.
- [21] H.Y. Luo, D.F. Consoli, W.R. Gunther, Y. Román-Leshkov, Investigation of the reaction kinetics of isolated Lewis acid sites in Beta zeolites for the Meerwein-Ponndorf-Verley reduction of methyl levulinate to  $\gamma$ -valerolactone, *J. Catal.* 320 (2014) 198–207.
- [22] V.L. Sushkevich, I.I. Ivanova, S. Tolborg, E. Taarning, Meerwein-Ponndorf-Verley-Oppenauer reaction of crotonaldehyde with ethanol over Zr-containing catalysts, *J. Catal.* 316 (2014) 121–129.
- [23] J.M. Hidalgo, C. Jiménez-Sanchidrián, J.R. Ruiz, Delaminated layered double hydroxides as catalysts for the Meerwein-Ponndorf-Verley reaction, *Appl. Catal. A: Gen.* 470 (2014) 311–317.
- [24] J. Song, B. Zhou, H. Zhou, L. Wu, Q. Meng, Z. Liu, B. Han, Porous zirconium-phytic acid hybrid: a highly efficient catalyst for Meerwein-ponndorf-verley reductions, *Angew. Chem. Int. Ed.* 54 (2015) 9399–9403.
- [25] F. Gonell, M. Boronat, A. Corma, Structure-reactivity relationship in isolated Zr sites present in Zr-zeolite and  $\text{ZrO}_2$  for the Meerwein-Ponndorf-Verley reaction, *Catal. Sci. Technol.* 7 (2017) 2865–2873.
- [26] X. Tang, H. Chen, L. Hu, W. Hao, Y. Sun, X. Zeng, L. Lin, S. Liu, Conversion of biomass to  $\gamma$ -valerolactone by catalytic transfer hydrogenation of ethyl levulinate over metal hydroxides, *Appl. Catal. B: Environ.* 147 (2014) 827–834.
- [27] M. Koehle, R.F. Lobo, Lewis acidic zeolite beta catalyst for the Meerwein-Ponndorf-Verley reduction of furfural, *Catal. Sci. Technol.* 6 (2015) 3018–3026.
- [28] A.H. Velekar, K.-H. Cho, S.K. Chitale, D.-Y. Hong, G.-Y. Cha, U.-H. Lee, D. Hwang, C. Serre, J.S. Chang, Y.-K. Hwang, Catalytic transfer hydrogenation of ethyl levulinate to  $\gamma$ -valerolactone over zirconium-based metal-organic frameworks, *Green Chem.* 18 (2016) 4542–4552.
- [29] Y. Zhu, S. Jaenicke, G.K. Chuah, Supported zirconium propoxide—a versatile heterogeneous catalyst for the Meerwein-Ponndorf-Verley reduction, *J. Catal.* 218 (2003) 396–404.
- [30] H. Li, Z. Fang, J. He, S. Yang, Ordered layered Zr-benzylphosphonate nanohybrids for efficient acid-base-mediated bifunctional/cascade catalysis, *ChemSusChem* 10 (2016) 681–686.
- [31] H. Li, J. He, A. Riisager, S. Saravananuragan, B. Song, S. Yang, Acid-base bifunctional zirconium *n*-alkyltriphosphate nanohybrid for hydrogen transfer of biomass-derived carboxides, *ACS Catal.* 6 (2016) 7722–7727.
- [32] J. Song, L. Wu, B. Zhou, H. Zhou, H. Fan, Y. Yang, Q. Meng, B. Han, A new porous Zr-containing catalyst with a phenate group: an efficient catalyst for the catalytic transfer hydrogenation of ethyl levulinate to  $\gamma$ -valerolactone, *Green Chem.* 17 (2015) 1626–1632.
- [33] Z. Xue, J. Jiang, G. Li, W. Zhao, J. Wang, T. Mu, Zirconium-cyanuric acid coordination polymer: highly efficient catalyst for conversion of levulinic acid to  $\gamma$ -valerolactone, *Catal. Sci. Technol.* 6 (2016) 5374–5379.
- [34] Y. Sha, Z. Xiao, H. Zhou, K. Yang, Y. Song, N. Li, R. He, K. Zhi, Q. Liu, Direct use of humic acid mixtures to construct efficient Zr-containing catalysts for Meerwein-Ponndorf-Verley reactions, *Green Chem.* 19 (2017) 4829–4837.
- [35] H. Li, X. Liu, T. Yang, W. Zhao, S. Saravananuragan, S. Yang, Porous zirconium-furandicarboxylate microspheres for efficient redox conversion of biofurans, *ChemSusChem* 10 (2017) 1761–1770.
- [36] H. Li, T. Yang, Z. Fang, Biomass-derived mesoporous Hf-containing hybrid for efficient Meerwein-Ponndorf-Verley reduction at low temperatures, *Appl. Catal. B: Environ.* 227 (2018) 79–89.
- [37] M. Saidi, F. Samimi, D. Karimipourfard, T. Nimmanwudipong, B.C. Gates, M.R. Rahimpour, Upgrading of lignin-derived bio-oils by catalytic hydrodeoxygenation, *Energy Environ. Sci.* 7 (2013) 103–129.
- [38] F. Li, X. Wang, T. Yuan, R.C. Sun, Lignosulfonate-modified graphene hydrogel with ultrahigh adsorption capacity for Pb(II) removal, *J. Mater. Chem. A* 4 (2016) 11888–11896.
- [39] Z. Ding, F. Li, J.L. Wen, X. Wang, R.C. Sun, Gram-scale synthesis of single-crystalline graphene quantum dots derived from lignin biomass, *Green Chem.* 20 (2018) 1383–1390.
- [40] L.J. Konwar, A. Samikannu, P. Mäki-Arvela, B. Dan, J.P. Mikkola, Lignosulfonate-based macro/mesoporous solid protonic acids for acetalization of glycerol to bio-additives, *Appl. Catal. B: Environ.* 220 (2017) 314–323.
- [41] S.S. Li, L. Ning, G.Y. Li, L. Lin, A.Q. Wang, C. Yu, X.D. Wang, Z. Tao, Lignosulfonate-based acidic resin for the synthesis of renewable diesel and jet fuel range alkanes with 2-methylfuran and furfural, *Green Chem.* 17 (2015) 3644–3652.
- [42] J. Iglesias, J.A. Melero, G. Morales, Y. Moreno, Y. Segura, M. Paniagua, A. Cambra, B. Hernández, Zr-SBA-15 Lewis acid catalyst: activity in Meerwein-Ponndorf-Verley reduction, *Catalysts* 5 (2015) 1911–1927.
- [43] M. Thommes, K. Kaneko, A.V. Neimark, J.P. Olivier, F. Rodriguez-Reinoso, J. Rouquerol, K.S.W. Sing, Physisorption of gases, with special reference to the evaluation of surface area and pore size distribution (IUPAC Technical Report), *Pure Appl. Chem.* 87 (2015) 1051–1069.
- [44] L.J. Konwar, A. Samikannu, P. Mäki-Arvela, J.P. Mikkola, Efficient C–C coupling of bio-based furanics and carbonyl compounds to liquid hydrocarbon precursors over lignosulfonate derived acidic carbocatalysts, *Catal. Sci. Technol.* 8 (2018) 2449–2459.
- [45] B. Xiao, X. Sun, R. Sun, Chemical, structural, and thermal characterizations of alkali-soluble lignins and hemicelluloses, and cellulose from maize stems, rye straw, and rice straw, *Polym. Degrad. Stab.* 74 (2001) 307–319.
- [46] P. Bansal, G.R. Chaudhary, S.K. Mehta, Comparative study of catalytic activity of  $\text{ZrO}_2$  nanoparticles for sonocatalytic and photocatalytic degradation of cationic and anionic dyes, *Chem. Eng. J.* 280 (2015) 475–485.
- [47] Y. Kuwahara, W. Kaburagi, T. Fujitani, Catalytic transfer hydrogenation of levulinic esters to  $\gamma$ -valerolactone over supported ruthenium hydroxide catalysts, *RSC Adv.* 4 (2014) 45848–45855.
- [48] V.A. Ivanov, J. Bachelier, F. Audry, J.C. Lavalley, Study of the Meerwein-Ponndorf-Verley reaction between ethanol and acetone on various metal oxides, *J. Mol. Catal.* 91 (1994) 45–59.
- [49] W. Gong, C. Chen, Y. Zhang, H. Zhou, H. Wang, H. Zhang, Y. Zhang, G. Wang, H. Zhao, Efficient synthesis of furfuryl alcohol from  $\text{H}_2$ -hydrogenation/transfer hydrogenation of furfural using sulfonate group modified Cu catalyst, *ACS Sustain. Chem. Eng.* 5 (2017) 2172–2180.
- [50] R.J. Chimentão, H. Oliva, J. Belmar, K. Morales, P. Mäki-Arvela, J. Wärnå, D.Yu. Murzin, J.L.G. Fierro, J. Llorca, D. Ruiz, Selective hydrodeoxygenation of biomass derived 5-hydroxymethylfurfural over silica supported iridium catalysts, *Appl. Catal. B: Environ.* 241 (2019) 270–283.
- [51] E. García-Sancho, I. Fúnez-Núñez, R. Moreno-Tost, J. Santamaría-González, E. Pérez-Inestrosa, J.L.G. Fierro, P. Maireles-Torres, Beneficial effects of calcium chloride on glucose dehydration to 5-hydroxymethylfurfural in the presence of

- alumina as catalyst, *Appl. Catal. B: Environ.* 206 (2017) 617–625.
- [52] I. Jiménez-Morales, M. Moreno-Recio, J. Santamaría-González, P. Maireles-Torres, A. Jiménez-López, Mesoporous tantalum oxide as catalyst for dehydration of glucose to 5-hydroxymethylfurfural, *Appl. Catal. B: Environ.* 154 (2014) 190–196.
- [53] M. Balakrishnan, E.R. Sacia, A.T. Bell, Etherification and reductive etherification of 5-(hydroxymethyl)furfural: 5-(alkoxymethyl)furfurals and 2,5-bis(alkoxymethyl)furans as potential bio-diesel candidates, *Green Chem.* 14 (2012) 1626–1634.
- [54] J.D. Lewis, S. Van De Vyver, A.J. Crisci, W.R. Gunther, V.K. Michaelis, R.G. Griffin, Y. Román-Leshkov, A continuous flow strategy for the coupled transfer hydrogenation and etherification of 5-(hydroxymethyl)furfural using Lewis acid zeolites, *ChemSusChem* 7 (2014) 2255–2265.
- [55] M.J. Gilkey, P. Panagiotopoulou, A.V. Mironenko, G.R. Jenness, D.G. Vlachos, B. Xu, Mechanistic insights into metal Lewis acid-mediated catalytic transfer hydrogenation of furfural to 2-methylfuran, *ACS Catal.* 5 (2015) 3988–3994.
- [56] C. Xie, J. Song, B. Zhou, J. Hu, Z. Zhang, P. Zhang, Z. Jiang, B. Han, Porous hafnium phosphonate: novel heterogeneous catalyst for conversion of levulinic acid and esters into  $\gamma$ -valerolactone, *ACS Sustain. Chem. Eng.* 4 (2016) 6231–6236.